THE JOURNAL OF BIOLOGICAL CHEMISTRY VOL. 289, NO. 24, pp. 16914–16923, June 13, 2014

Structural Basis for Calcium and Magnesium Regulation of a Large Conductance Calcium-activated Potassium Channel with β1 Subunits*

Received for publication, February 13, 2014, and in revised form, April 21, 2014 Published, JBC Papers in Press, April 24, 2014, DOI 10.1074/jbc.M114.557991

Hao-Wen Liu[‡1], Pan-Pan Hou[‡1], Xi-Ying Guo[‡1], Zhi-Wen Zhao[‡], Bin Hu[‡], Xia Li[‡], Lu-Yang Wang[§], Jiu-Ping Ding[‡2], and Sheng Wang[‡3]

From the [‡]Key Laboratory of Molecular Biophysics of the Ministry of Education, College of Life Science and Technology, Huazhong University of Science and Technology, Wuhan, Hubei 430074, China and the [§]Program in Neurosciences and Mental Health, SickKids Research Institute and Department of Physiology, University of Toronto, Toronto, Ontario M5G 1X8, Canada

Background: Large conductance calcium-activated potassium (BK) channels are regulated by β1 subunits.
Results: We identified two binding sites engaged in intersubunit interactions to regulate the sensitivity of BK to divalent ions.
Conclusion: Both electrostatic and hydrophobic sites enhance the calcium sensitivity of BK, whereas the hydrophobic site selectively reduces the magnesium sensitivity.
Significance: This work provides structural and mechanistic insights into the molecular mechanism of BK(β1) gating.

Large conductance Ca^{2+}- and voltage-activated potassium (BK) channels, composed of pore-forming α subunits and auxiliary β subunits, play important roles in diverse physiological activities. The β1 is predominately expressed in smooth muscle cells, where it greatly enhances the Ca^{2+} sensitivity of BK channels for proper regulation of smooth muscle tone. However, the structural basis underlying dynamic interaction between BK mSlo1 α and β1 remains elusive. Using macroscopic ionic current recordings in various Ca^{2+} and Mg^{2+} concentrations, we identified two binding sites on the cytosolic N terminus of β1, namely the electrostatic enhancing site (mSlo1(K392,R393)-β1(E13,T14)), increasing the calcium sensitivity of BK channels, and the hydrophobic site (mSlo1(L906,L908)-β1(L5,V6,M7)), passing the physical force from the Ca^{2+} bowl onto the enhancing site and S6 C-linker. Dynamic binding of these sites affects the interaction between the cytosolic domain and voltage-sensing domain, leading to the reduction of Mg^{2+} sensitivity. A comprehensive structural model of the BK(mSlo1 α-β1) complex was reconstructed based on these functional studies, which provides structural and mechanistic insights for understanding BK gating.

BK[4] channels play critical roles in modulating many physiological activities, such as neurotransmitter release and endocrine secretion in neurons or endocrine cells, contraction of smooth muscle cells, and even frequency tuning in hair cells (1–5). These large conductance channels exhibit a considerable functional diversity with respect to their kinetic behavior, apparent Ca^{2+} and Mg^{2+} regulation, and pharmacological sensitivity to toxins (6, 7). The cytosolic domain (CTD) of the BK channel contains multiple divalent ion binding sites, including two Ca^{2+} binding sites with high and moderate affinity respectively as well as a low affinity Mg^{2+} binding site (8–10). Functional heterogeneity of native BK-type channels is often imparted by their association with tissue-specific auxiliary β1–β4 subunits. For example, the mSlo1 α subunits and β1 subunits are mostly co-localized in smooth muscle cells in heart and vascular tissues (11–13). These auxiliary subunits share a similar topology of two transmembrane (TM1 and TM2) segments, intracellular N and C termini, and a large extracellular loop (14–18). One BK channel can associate with up to four auxiliary β subunits in 1:1 stoichiometry with mSlo1 α subunits (19, 20). The β1 and β2 subunits of the β family share the highest sequence homology and increase the apparent Ca^{2+} sensitivity of BK channels (15, 19, 20). Several laboratories have reported that magnesium is also able to activate BK channels at the mSlo1(E374,E399) sites (9, 10), and the locus of the Mg^{2+} binding domain resides in the cytosolic terminal of S4 between the voltage-sensing domain (VSD) and the first C-terminal regulators of K^+ conductance (RCK1) (21). Previous studies have reported that Mg^{2+} sensitivity of BK is attenuated by β1 (22) and subsequently by β2 but to different extent (23). These reports imply that β subtype-dependent differences in the sensitivity to Ca^{2+} and Mg^{2+} are possibly derived from their distinct structures.

Compared with the β2, the β1 only modifies the BK activation without affecting inactivation and rectification, probably due to a lack of the inactivation domain at its N terminus and basic residues distributed around the outer pore (24, 25). Fur-

* This work was supported by National Basic Research Program of China Grant 2010CB529804 (to J. P. D.); Fundamental Research Funds for the Central Universities Grant 2014TS087 (to S. W.); National Science Foundation of China Grants 30971179, 31170814, and 31028006 (to J. P. D.); and individual Operating Grants from the Canadian Institutes of Health Research, a China-Canada Joint Health Research Initiative grant, and the Canada Research Chair (to L. Y. W.).
[1] These authors contributed equally to this work.
[2] To whom correspondence may be addressed. Tel.: 86-27-877-921-53; Fax: 86-27-877-920-24; E-mail: jpding@mail.hust.edu.cn.
[3] To whom correspondence may be addressed. Tel.: 86-27-877-921-53; Fax: 86-27-877-920-24; E-mail: shengwang@mail.hust.edu.cn.
[4] The abbreviations used are: BK, large conductance voltage- and Ca^{2+}-activated potassium; E site, enhancing site; H site, hydrophobic site; VSD, voltage-sensing domain; CTD, cytosolic domain; PGD, pore-gating domain; TM, transmembrane; mSlo1(5D5N), mSlo1(D898N/D899N/D900N/D901N/D903N).

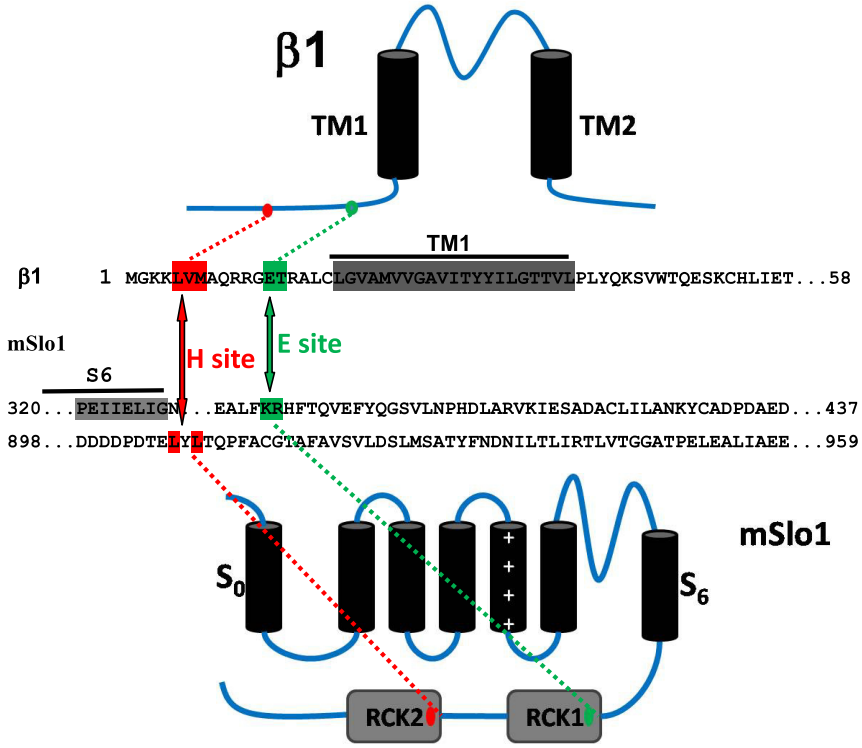

FIGURE 1. **An interaction schematic of mutations of mSlo1 and β1 subunits.** Topological interaction maps between mutations of mSlo1 α (*bottom*) and β1 subunits (*top*) are displayed. The *central panel* denotes a partial sequence of β1 and mSlo1. The *colored* amino acids (*red* and *green*) in mSlo1 and in the N terminus of β1 are the regions of α/β interaction, termed the H and E sites, as indicated.

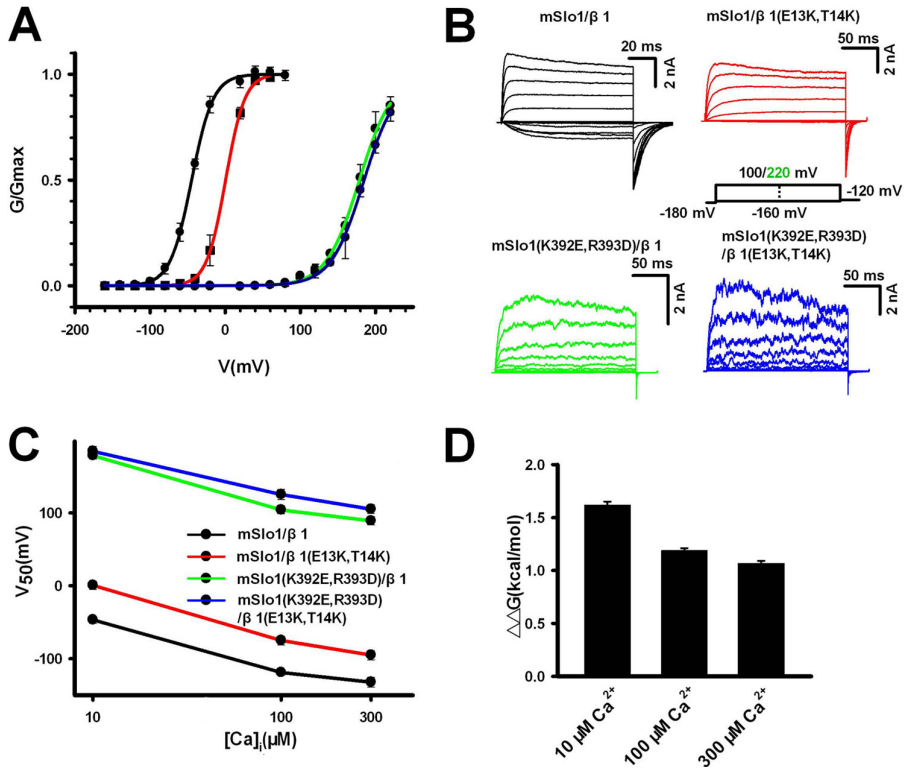

FIGURE 2. **Electrostatic interaction between mSlo1(K392,R393) and β1(E13,T14) determined by double mutant cycle analysis.** *A*, *G-V* curves were plotted for mSlo1-β1 (V_{50} = −46.7 ± 4.8 mV, n = 10; *black*), mSlo1-β1(E13K,T14K) (V_{50} = 0.7 ± 5.5 mV, n = 9; *red*), mSlo1(K392E,R393D)-β1 (V_{50} = 178.3 ± 4.9 mV, n = 7; *green*), and mSlo1(K392E,R393D)-β1(E13K,T14K) (V_{50} = 189.0 ± 6.5 mV, n = 6; *blue*). *Solid lines* are single Boltzmann functions fitted to each *G-V* curve. *B*, representative currents from each experimental combination, recorded from inside-out patches, activated by voltage steps from −160 mV through 100/200 mV in increments of 20 mV, as indicated, after a prepulse of −180 mV, in 10 μM Ca^{2+}. *C*, the values of V_{50} were obtained in 10, 100, and 300 μM Ca^{2+}, respectively. *D*, the ΔΔ*G* values of mSlo1(K392E,R393D) *versus* β1(E13K,T14K) are 1.62 ± 0.03, 1.17 ± 0.02, and 1.07 ± 0.02 kcal/mol in 10, 100, and 300 μM Ca^{2+}, respectively. *Error bars*, S.D.

thermore, the β2 subunit has been identified to interact with the N terminus, including the S0 segment of Slo1 and the AC region (βA-αC) of the RCK1 domain (21), and the exact binding sites between the mSlo1 α and β2 subunits have recently been identified (26). Several reports reveal that the N terminus and S0 segment play an important role in the function of β1 subunit (27, 28). Cross-linking experiments show that the intracellular end of β1 TM2 and mSlo1 α S0 are in contact and that the intracellular end of β1 TM1 is close to both mSlo1 α S1 and S2 (29). Chimera experiments demonstrated that the intracellular domains were crucial for functions of the β1 subunit (30). However, the detailed intracellular interaction sites between the mSlo1 α and β1 subunits remain unknown.

In order to determine the intracellular activation sites between the mSlo1 α and β1 subunits, we used double mutant cycle analysis to examine interaction based on the changes of free energy between the potential coupling residues. We found two crucial interaction sites on β1, namely an electrostatic enhancing (E) site and a hydrophobic (H) site in the cytosolic region for its coupling to mSlo1 α. We further constructed a computational model of the mSlo1-β1 channel complex in the context of its structural and functional feasibility. Altogether, our results provided a putative working model of the mSlo1-β1 complex, capable to explain both the Ca^{2+} and Mg^{2+} sensitivity of BK(β1) channels.

TABLE 1

Gating kinetics of mutated BK channels

The first column shows the mutated BK type channels. The activation (τ_{act}) and deactivation (τ_{dea}) time constants were calculated at 100 mV except for mSlo1(K392E,R393D)-β1 and mSlo1(K392E,R393D)-β1(E13K,T14K), which were calculated at 200 mV, respectively.

BK channel	τ_{act}	τ_{dea}
	ms	*ms*
mSlo1-β1	2.4 ± 0.4	10 ± 0.8
mSlo1-β1(E13K,T14K)	4.0 ± 0.6	4.5 ± 0.6
mSlo1(K392E,R393D)-β1	4.2 ± 0.7 (200 mV)	0.78 ± 0.2 (200 mV)
mSlo1(K392E,R393D)-β1 (E13K,T14K)	3.8 ± 0.4 (200 mV)	0.85 ± 0.2 (200 mV)
mSlo1-β1(L5Q,V6Q,M7Q)	7.4 ± 0.8	5.2 ± 0.5
mSlo1(L906Q,L908Q)-β1	15 ± 1.5	5.0 ± 0.4
mSlo1(L906Q,L908Q)-β1 (L5Q,V6Q,M7Q)	60 ± 3.4	1.4 ± 0.2
mSlo1-β1(K3Q,K4Q)	2.4 ± 0.3	7.4 ± 0.8
mSlo1(5D5N)-β1	13 ± 1.0	1.7 ± 0.3
mSlo1(5D5N)-β1(K3Q,K4Q)	30 ± 2.4	2.3 ± 0.4

EXPERIMENTAL PROCEDURES

Constructs and Mutations—All α-subunit constructs were made from the *mbr5* splice variant of mouse Slo1 (KCNMA1; GenBank™ accession number L16912). Human β1 (KCNMB1; GenBank™ accession number U25138.1) cDNAs were subcloned into pcDNA3.1. Mutations were introduced using the QuikChange site-directed mutagenesis kit (Stratagene). Specifically, the mutant mSlo1(D898N/D899N/D900N/D901N/D903N) (mSlo1(5D5N)) in the calcium bowl of RCK2 was constructed. All constructs and point mutations were verified by direct DNA sequence analysis. Fig. 1 shows the topological map of the constructs and mutations for all of the experiments.

Cell Culture and Transient Transfections in HEK293 Cells—HEK293 cells were cultured in DMEM supplemented with 10% fetal bovine serum (FBS), 100 units/ml penicillin, and streptomycin in incubators with 37 °C and 5% CO_2. One day before transfection, cells were transferred to 24-well plates. At 90% confluence, transfections could be performed with Lipofectamine 2000 (Invitrogen). 4–6 h after transfection, the cells were transferred to a poly-D-lysine (Sigma)-coated slide for the patch clamp recordings. For all of the co-transfections, the ratio of α to β subunits was 1:2.

Patch Clamp Recording—For recordings, transfected HEK293 cells were transferred 1 day after transfection to 160 K^+ solution containing 160 mM $MeSO_3K$, 2 mM $MgCl_2$, 10 mM HEPES (pH 7.0). All experiments were carried out with excised patches, in inside-out recording configuration. Patch pipettes were

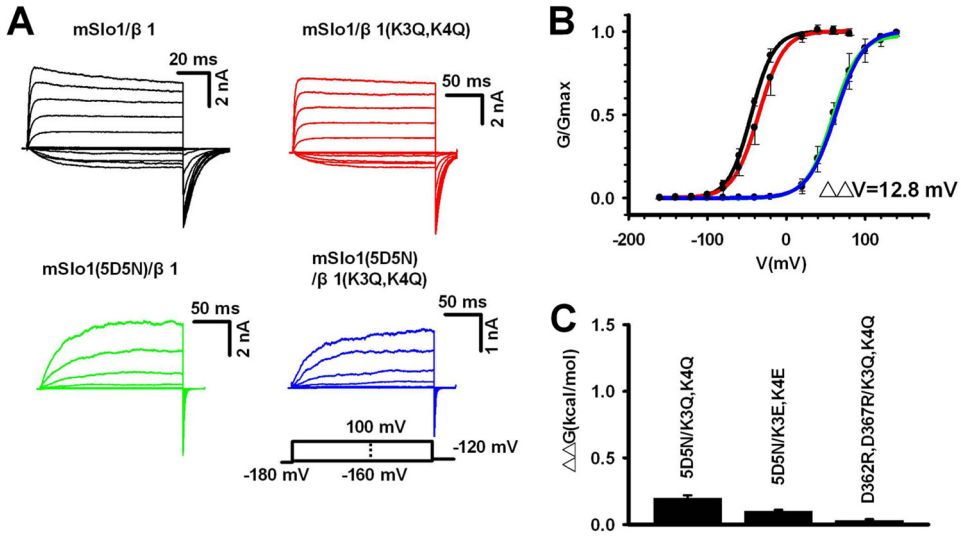

FIGURE 3. **There was no electrostatic interaction between the calcium binding sites and β1(K3,K4).** *A*, representative currents from each experimental combination, recorded from inside-out patches, activated by voltage steps from −160 mV through 100 mV in increments of 20 mV, as indicated, after a prepulse of −180 mV, in 10 μM Ca^{2+}. *B*, *G-V* curves were plotted for mSlo1-β1 (V_{50} = −46.7 ± 4.8 mV, *n* = 10; *black*), mSlo1-β1(K3Q,K4Q) (V_{50} = −35.1 ± 5.6 mV, *n* = 8; *red*), mSlo1(5D5N)-β1 (V_{50} = 59.1 ± 4.9 mV, *n* = 7; *green*), and mSlo1(5D5N)-β1(K3Q,K4Q) (V_{50} = 62.4 ± 6.0 mV, *n* = 7; *blue*). *Solid lines*, single Boltzmann functions fitted to each *G-V* curve. *C*, the values of ΔΔ*G* were plotted for mSlo1(5D5N)-β1(K3Q,K4Q), mSlo1(5D5N)-β1(K3E,K4E), and mSlo1(D362R,D367R)-β1(K3Q,K4Q). Their values of ΔΔ*G* are 0.3 ± 0.02 kcal/mol for mSlo1(5D5N)-β1(K3Q,K4Q), 0.2 ± 0.02 kcal/mol for mSlo1(5D5N)-β1(K3E,K4E), and 0.1 ± 0.02 kcal/mol for mSlo1(D362R,D367R)-β1(K3Q,K4Q), as indicated. *Error bars*, S.D.

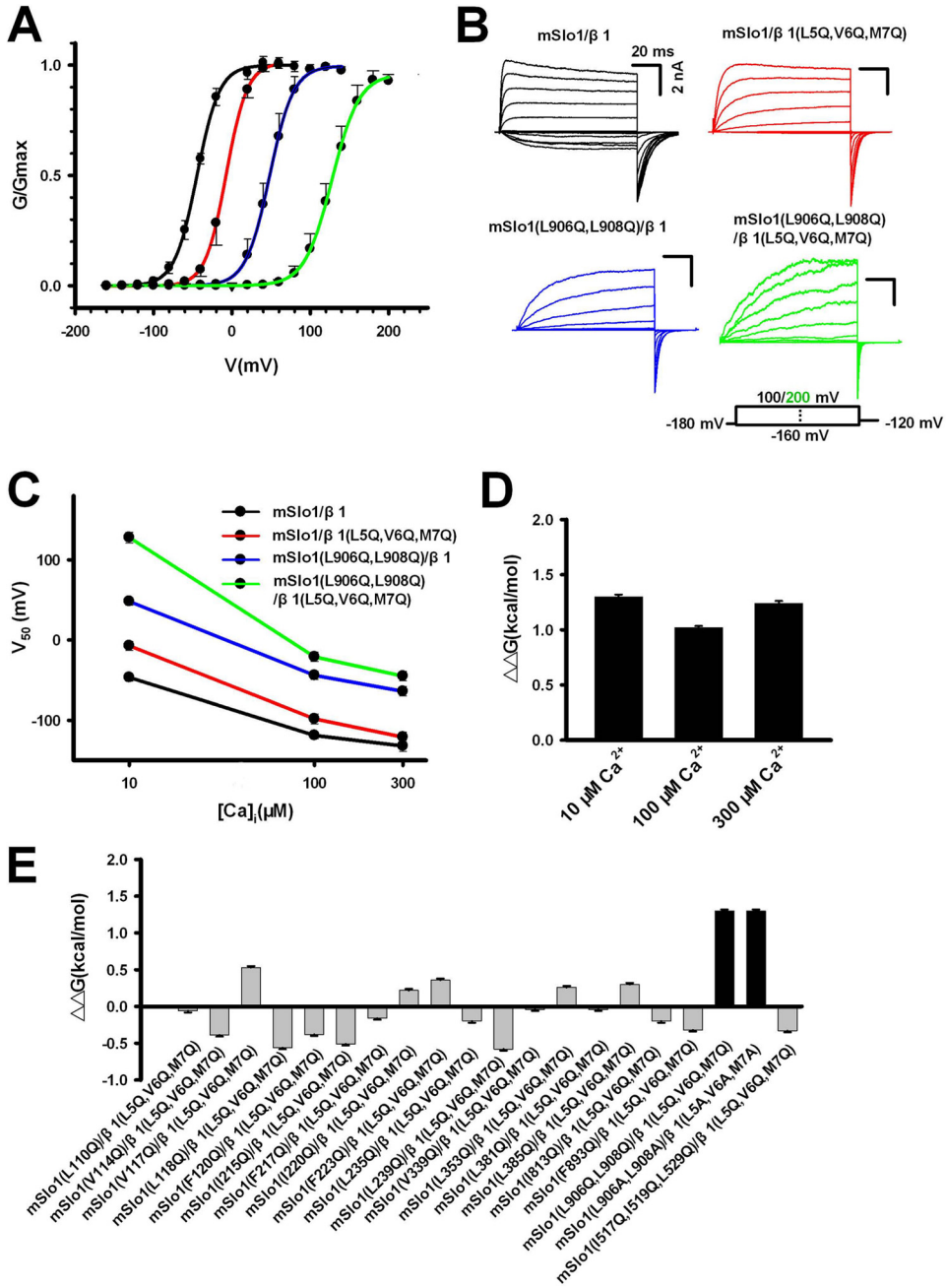

FIGURE 4. **The hydrophobic interaction between mSlo1(L906,L908) and β1(L5,V6,M7).** *A*, representative currents from each experimental combination, recorded from inside-out patches, activated by voltage steps from −160 mV through 100/200 mV in increments of 20 mV, as indicated, after a prepulse of −180 mV, in 10 μM Ca^{2+}. *B*, *G-V* curves are plotted for mSlo1-β1 (V_{50} = −46.7 ± 4.8 mV, *n* = 10; *black*), mSlo1-β1(L5Q,V6Q,M7Q) (V_{50} = −7.2 ± 5.6 mV, *n* = 11; *red*), mSlo1(L906Q,L908Q)-β1 (V_{50} = 48.2 ± 4.8 mV, *n* = 7; *blue*), and mSlo1(L906Q,L908Q)-β1(L5Q,V6Q,M7Q) (V_{50} = 127.7 ± 5.8 mV, *n* = 8; *green*). *Solid lines*, single Boltzmann functions fitted to each *G-V* curve. *C*, their values of V_{50} were obtained in 10, 100, and 300 μM Ca^{2+}, as indicated. *D*, the values of ΔΔ*G* of mSlo1(L906Q,L908Q)-β1(L5Q,V6Q,M7Q) are 1.30 ± 0.02, 1.05 ± 0.02, and 1.24 ± 2.4 kcal/mol in 10, 100, and 300 μM Ca^{2+}, respectively. *E*, the values of ΔΔ*G* were plotted for mSlo1 mutations *versus* β1(LVM) at 10 μM Ca^{2+}, as indicated. The ΔΔ*G* of mSlo1(L906,L908)-β1(L5,V6,M7) is 1.30 ± 0.02 kcal/mol, and this was only identified as a pair of binding sites based on its ΔΔ*G* (>1 kcal/mol). *Error bars*, S.D.

pulled from borosilicate glass capillaries with resistances of 2–3 megaohms when filled with pipette solution. Experiments were performed using an Axopatch 200B patch clamp amplifier with its software (Axon). Currents were typically digitized at 20 kHz and filtered at 8.5 kHz. During recording, different Ca^{2+} and Mg^{2+} concentration solutions were applied onto membrane patches via a perfusion pipette containing eight solution channels. The 0 mM Mg^{2+} solution contained 160 mM $MeSO_3K$, 10 mM $MgCl_2$, 5 mM EGTA, 10 HEPES (pH 7.0). All experiments were performed at room temperature (22–24 °C).

Homology Modeling—The full models of BK channel were built by homology modeling combination with the known partial crystal structure of ion channels (*i.e.* RCK domains), and then the complex of mSlo1 and hβ1 were assembled manually. During the modeling process, the S1-S6 domains were built from MthK (Protein Data Bank entry 1LNQ) and KcSA (Pro-

TABLE 2

Influence of mutations on BK channels

The first column shows the corresponding mutations of BK channels. Estimates for the values of V_{50} and Z for the different mutations were obtained by fitting G-V curves to the Boltzmann equation. The free energy is given by $-ZFV_{50}$.

BK channel	V_{50}	Z	$-ZFV_{50}$
	mV		*kcal/mol*
mSlo1-β1	−46.7 ± 4.8	1.70 ± 0.21	1.83 ± 0.02
mSlo1-β1(E13K,T14K)	0.7 ± 3.2	2.07 ± 0.17	0.03 ± 0.01
mSlo1(K392D,R393D)-β1	178.3 ± 6.2	1.16 ± 0.15	−4.79 ± 0.02
mSlo1(K392D,R393D)-β1(E13K,T14K)	184.2 ± 6.5	1.17 ± 0.16	−4.97 ± 0.02
mSlo1-β1(L5Q,V6Q,M7Q)	−7.2 ± 5.5	1.70 ± 0.15	0.28 ± 0.02
mSlo1-β1(L5Q)	−33.5 ± 5.2	1.70 ± 0.13	1.32 ± 0.02
mSlo1-β1(V6Q)	−18.5 ± 5.1	1.69 ± 0.14	0.71 ± 0.02
mSlo1-β1(M7Q)	−20.4 ± 4.9	1.70 ± 0.15	0.80 ± 0.02
mSlo1(L906Q,L908Q)-β1	46.7 ± 6.1	1.74 ± 0.20	−1.88 ± 0.02
mSlo1(L906Q,L908Q)-β1(L5Q,V6Q,M7Q)	127.9 ± 6.4	1.64 ± 0.17	−4.86 ± 0.02
mSlo1-β1(L5A,V6A,M7A)	−7.0 ± 5.6	2.03 ± 0.22	0.33 ± 0.02
mSlo1(L906A,L908A)-β1	128.0 ± 6.2	1.24 ± 0.15	3.68 ± 0.02
mSlo1(L906A,L908A)-β1(L5A,V6A,M7A)	145.1 ± 6.1	1.16 ± 0.16	3.88 ± 0.02
mSlo1-β1(K3Q,K4Q)	−35.1 ± 4.7	1.60 ± 0.15	1.3 ± 0.01
mSlo1(5D5N)-β1	59.1 ± 4.9	1.51 ± 0.16	−2.07 ± 0.02
mSlo1(5D5N)-β1(K3Q,K4Q)	62.0 ± 6.1	1.44 ± 0.07	−2.08 ± 0.01
mSlo1(D362R,D367R)-β1	6.49 ± 5.0	1.74 ± 0.15	−0.26 ± 0.02
mSlo1(D362R,D367R)-β1(K3Q,K4Q)	18.3 ± 5.5	1.78 ± 0.13	−0.75 ± 0.02
mSlo1(L110Q)-β1	−63.2 ± 6.5	1.70 ± 0.08	2.48 ± 0.02
mSlo1(L110Q)-β1(L5Q,V6Q,M7Q)	−18.6 ± 5.1	2.02 ± 0.14	0.87 ± 0.02
mSlo1(V114Q)-β1	−13.2 ± 6.0	1.74 ± 0.08	0.53 ± 0.02
mSlo1(V114Q)-β1(L5Q,V6Q,M7Q)	38.4 ± 5.8	1.59 ± 0.12	−1.41 ± 0.02
mSlo1(V117Q)-β1	−81.2 ± 6.5	1.52 ± 0.14	2.86 ± 0.20
mSlo1(V117Q)-β1(L5Q,V6Q,M7Q)	−45.6 ± 5.3	1.74 ± 0.10	1.84 ± 0.01
mSlo1(L118Q)-β1	−70 ± 5.2	1.82 ± 0.13	2.94 ± 0.02
mSlo1(L118Q)-β1(L5Q,V6Q,M7Q)	−21.3 ± 5.5	1.68 ± 0.09	0.83 ± 0.01
mSlo1(F120Q)-β1	−37.5 ± 4.8	1.67 ± 0.14	1.45 ± 0.02
mSlo1(F120Q)-β1(L5Q,V6Q,M7Q)	11.7 ± 5.6	1.78 ± 0.12	−0.48 ± 0.02
mSlo1(I215Q)-β1	−18.2 ± 6.5	1.74 ± 0.06	0.73 ± 0.01
mSlo1(I215Q)-β1(L5Q,V6Q,M7Q)	35.4 ± 4.5	1.62 ± 0.10	−1.33 ± 0.01
mSlo1(F217Q)-β1	−78.7 ± 6.4	1.84 ± 0.11	3.36 ± 0.02
mSlo1(F217Q)-β1(L5Q,V6Q,M7Q)	−38.5 ± 5.2	1.86 ± 0.12	1.65 ± 0.02
mSlo1(I220Q)-β1	−186.8 ± 6.8	0.85 ± 0.22	3.66 ± 0.03
mSlo1(I220Q)-β1(L5Q,V6Q,M7Q)	−152.2 ± 5.7	0.78 ± 0.15	2.73 ± 0.02
mSlo1(F223Q)-β1	−135.1 ± 5.5	0.95 ± 0.12	2.97 ± 0.02
mSlo1(F223Q)-β1(L5Q,V6Q,M7Q)	−71.5 ± 5.6	1.08 ± 0.11	1.78 ± 0.02
mSlo1(L235Q)-β1	41.5 ± 4.9	1.12 ± 0.13	−1.07 ± 0.02
mSlo1(L235Q)-β1(L5Q,V6Q,M7Q)	74 ± 6.5	1.54 ± 0.09	−2.64 ± 0.02
mSlo1(L239Q)-β1	−21.7 ± 5.4	1.62 ± 0.12	0.81 ± 0.02
mSlo1(L239Q)-β1(L5Q,V6Q,M7Q)	35.2 ± 6.1	1.62 ± 0.08	−1.32 ± 0.01
mSlo1(V339Q)-β1	−47.8 ± 4.8	1.70 ± 0.13	1.88 ± 0.01
mSlo1(V339Q)-β1(L5Q,V6Q,M7Q)	−6.7 ± 4.5	1.70 ± 0.10	0.26 ± 0.01
mSlo1(L353Q)-β1	−35.5 ± 5.1	1.82 ± 0.12	1.49 ± 0.02
mSlo1(L353Q)-β1(L5Q,V6Q,M7Q)	−4.7 ± 4.6	1.82 ± 0.13	0.2 ± 0.01
mSlo1(L381Q)-β1	−45.5 ± 4.8	1.70 ± 0.09	1.79 ± 0.01
mSlo1(L381Q)-β1(L5Q,V6Q,M7Q)	−5.1 ± 5.0	1.68 ± 0.12	0.20 ± 0.02
mSlo1(L385Q)-β1	50.1 ± 5.7	1.66 ± 0.13	−1.93 ± 0.02
mSlo1(L385Q)-β1(L5Q,V6Q,M7Q)	94.5 ± 6.5	1.45 ± 0.15	−3.18 ± 0.02
mSlo1(I517Q,I519Q,L529Q)-β1	12.2 ± 5.5	1.72 ± 0.12	−0.49 ± 0.02
mSlo1(I517Q,I519Q,L529Q)-β1(L5Q,V6Q,M7Q)	59.1 ± 5.5	1.72 ± 0.11	−2.37 ± 0.02
mSlo1(I813Q)-β1	−56.3 ± 5.7	1.68 ± 0.12	2.19 ± 0.02
mSlo1(I813Q)-β1(L5Q,V6Q,M7Q)	−11.5 ± 6.1	1.65 ± 0.13	0.44 ± 0.02
mSlo1(F893Q)-β1	18.5 ± 5.4	1.71 ± 0.09	−0.73 ± 0.01
mSlo1(F893Q)-β1(L5Q,V6Q,M7Q)	66.5 ± 6.5	1.69 ± 0.13	−2.60 ± 0.02

tein Data Bank entry 1K4C). The closed state RCK model was from previous reports (31, 32) (Protein Data Bank entry 3U6N). The S0 helix of BK and the TM1 of hβ1 was orientated manually according to another publication (29). The loosed loops of RCK and the linker of S0-S1 were also rebuilt and refined. The N-terminal 22-amino acid structure of β1 was constructed and refined by Amber12 with ff13 force field. First, the linear peptide was built with xleap of AmberTool13 and then minimized for 1000 steps, followed by 100,000 heating steps for 0–325 K; finally, 50,000,000 equilibration steps were taken for the whole ensemble. The simulation time is 50 ns to make the conformation more stable. During the whole construction process, the 22-amino acid peptide was put into implicit generalized Born solvent with 1-fs time step. Then the combination of 22-amino acid N terminus and TM1 helix of β1 subunit was constructed manually and put into a pre-equilibrated 1-palmitoyl-2-oleoyl-phosphatidylcholine membrane ensemble with explicit SPC water model and refined for another 50 ns by Molecular Dynamics Suite, Desmond version 3.6 (33). Similar to the BK(β2) complex, the combined model of full BK channel and partial β1 was assembled and embedded into an larger membrane ensemble with 1-palmitoyl-2-oleoyl-phosphatidylcholine, explicit SPC water model, and 160 mM KCl and then refined by a 5-ns standard molecular dynamics simulation with the Nosé-Hoover chain thermostat method and Martyna-Tobias-Klevin barostat method in Desmond version 3.6.

Data Analysis—Recording data were analyzed with Clampfit (Axon Instruments, Inc.) and Sigmaplot (SPSS, Inc.) software.

Unless otherwise stated, data are presented as mean ± S.D. *G-V* curves for activation were fitted by the single Boltzmann function with the form, $G/G_{max} = (1 + \exp((V - V_{50})/\kappa))^{-1}$, where V_{50} is the voltage at which the conductance (G) is half the maximum conductance (G_{max}), and κ is a factor affecting the steepness of the activations.

RESULTS

Determination of the Enhancing Site of mSlo1(β1) Channels—Both β1 and β2 subunits can enhance the Ca^{2+} sensitivity of BK channels (34–37). In previous work, we determined the complementary paired residues mSlo1(K392,R393)-β2(E44,D45) as an enhancing (E) site of BK (β2) channels (26). After comparing the sequences of β1 and β2, we found that a pair of conserved residues, β1(E13,T14), may play a role similar to that of β2(E44,D45). To explore the possible interaction between two groups of residues, we performed thermodynamic double mutant cycle analysis (38–41). Changes of free energy coupling between mutations in pairs of residues located in different subunits were respectively calculated by using a thermodynamic square composed of the WT complex (αβ), the two single mutants (α*β and αβ*), and the corresponding double mutant (α*β*) (asterisks denote a mutation). The thermodynamic square was described as follows, $\Delta\Delta G = \Delta G_{\alpha\beta^*} + \Delta G_{\alpha^*\beta} - \Delta G_{\alpha^*\beta^*}$. A distinct change of $\Delta\Delta G \geq 1$ kcal/mol would be judged to be coupled; otherwise it was not.

For double mutant cycle analyses, all *G-V* curves of the mSlo1(K392,R393) *versus* β1(E13,T14) cycle are shown in Fig. 2*A*. The corresponding currents, recorded from inside-out patches in 10 μM Ca^{2+}, are shown for each mutation (Fig. 2*B*). The values of V_{50} are −46.7 ± 4.8 mV for mSlo1-β1 (*black*); 0.7 ± 5.5 mV for mSlo1-β1(E13K,T14K) (*red*), which is close to the V_{50} of mSlo1 alone; 178.3 ± 4.9 mV for mSlo1(K392E,R393D)-β1 (*blue*); and 189.0 ± 6.5 mV for mSlo1(K392E,R393D)-β1(E13K,T14K) (*green*). The total change of $\Delta\Delta G$ is about 1.62 kcal/mol, suggesting that there is a strong coupling between the mSlo1(K392,R393) and β1(E13,T14). Similarly, additional experiments in 100 and 300 μM Ca^{2+} reinforce this observation (Fig. 2*C*). All of the statistics indicate that the $\Delta\Delta G$ for mSlo1(K392,R393) *versus* β1(E13,T14) is independent to Ca^{2+} (Fig. 2*D*).

Considering that both mSlo1(K392E,R393D) and β1(E13K,T14K) exhibited a significant change in kinetics of BK(β1) channel (Table 1) and that the mutant β1(E13K,T14K) abolished the calcium sensitivity of β1 (Fig. 2*C*), we conclude that the complementary paired residues mSlo1(K392,R393)-β1(E13,T14) form an E site.

Non-electrostatic Interaction between β1(K3,K4) and Calcium Binding Bowl—There are two different types of residues in the N terminus of the β1 subunit, namely electrostatic type-like β1(K3K4) and hydrophobic type-like β1(L5,V6,M7). There are many potential residues in the RCK domain of the BK α subunit that may couple with two types of binding sites, but we reason that two prerequisites must be satisfied: accessibility and associability. For the basic residues β1, the acidic ones in the RCK domain of BK α subunit near the β1(K3K4) are strong candidates, whereas the hydrophobic ones in the RCK domain probably bind to hydrophobic residues β1(L5,V6,M7).

In a previous study, we verified a calcium bowl site (*i.e.* mSlo1(calcium bowl)-β2(K33,R34,K35)) for the BK(β2) channel, which passes the original Ca^{2+} gating force from the calcium bowl to the E site (26). Based on the sequences of β1 and β2, we postulated that the residues β1(K3,K4) might also interact with mSlo1(calcium bowl) as β2(K33,R34,K35) did. To test this, we performed experiments based on double mutant cycle analysis. The representative currents, recorded from inside-out patches in 10 μM Ca^{2+}, were shown for each mutation (Fig. 3*A*). All of the *G-V* curves required for the mSlo1(5D5N) *versus* β1(K3,K4) cycle were shown in Fig. 3*B*. The values of V_{50} were −46.7 ± 4.8 mV for mSlo1-β1 (*black*), −35.1 ± 5.6 mV for mSlo1-β1(K3Q,K4Q) (*red*), 59.1 ± 4.9 mV for mSlo1(5D5N)-β1 (*blue*), and 62.4 ± 6.0 mV for mSlo1(5D5N)-β1(K3Q,K4Q) (*green*). The total $\Delta\Delta G$ was about 0.2 kcal/mol, suggesting that no significant interaction existed between the mSlo1(calcium bowl) and β1(K3,K4), differing from the case of mSlo1(calcium bowl) and β2(K33,R34,K35). Similar experiments were conducted for mSlo1(5D5N) *versus* β1(K3E,K4E). Our experiments showed that their $\Delta\Delta G$ was about 0.1 kcal/mol. It is

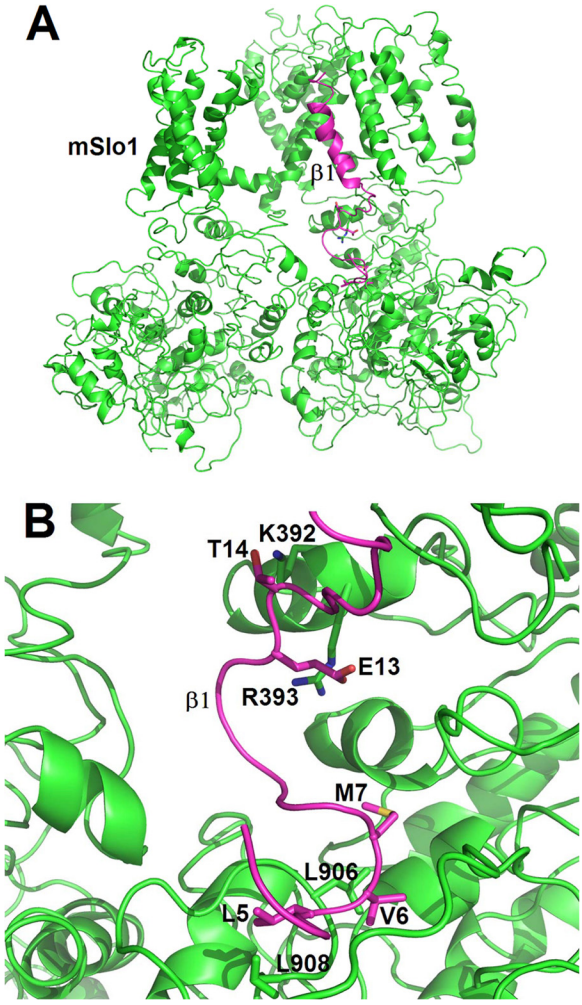

FIGURE 5. **A structural model for mSlo1 α interacting with the N terminus of β1.** *A*, *side view* of the mSlo1-β1 complex, composed of only two mSlo1 α subunits (*green*) associated with an N terminus-TM1 segment of β1 (*purple*), was drawn to show two pairs of residues (*i.e.* mSlo1(K392,R393)-β1(E13,T14) named as the E site and mSlo1(L906,L908)-β1(L5,V6,M7) named as the H site). *B*, the detailed spatial distribution of the above pairs of residues is shown. Both of the structural models were prepared and rendered by the PyMOL suite (PyMOL Molecular Graphics System, version 1.5.0.4, Schrodinger, LLC).

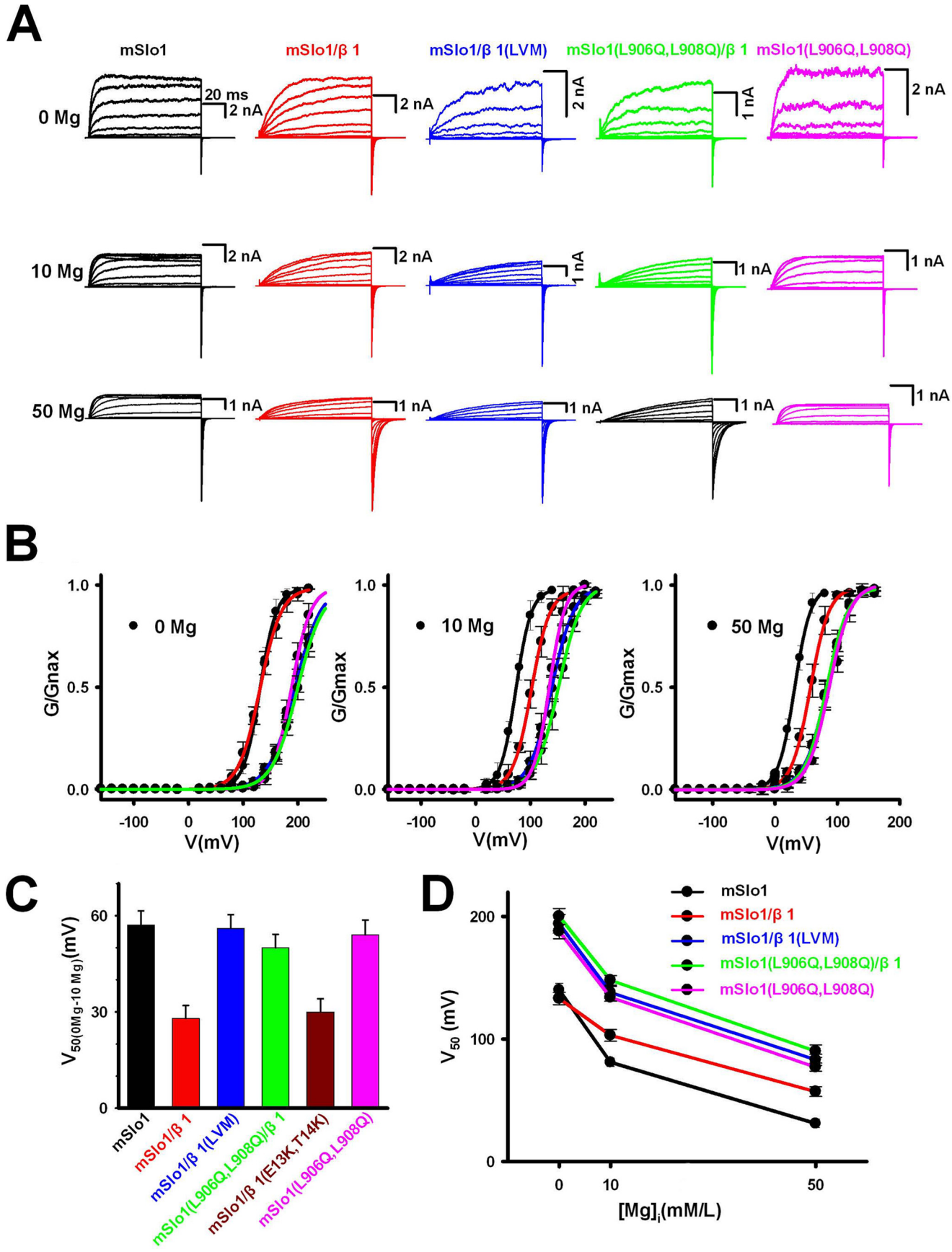
A
mSlo1
mSlo1/β 1
mSlo1/β 1(LVM)
mSlo1(L906Q,L908Q)/β 1
mSlo1(L906Q,L908Q)
0 Mg
10 Mg
50 Mg
20 ms
2 nA
1 nA
B
0 Mg
10 Mg
50 Mg
G/Gnax
G/Gmax
V(mV)
C
$V_{50(0Mg-10Mg)}$(mV)
mSlo1
mSlo1/β 1
mSlo1/β 1(LVM)
mSlo1(L906Q,L908Q)/β 1
mSlo1/β 1(E13K,T14K)
mSlo1(L906Q,L908Q)
D
V_{50} (mV)
[Mg]$_i$(mM/L)

nearly the same as that of mSlo1(5D5N) *versus* β1(K3Q,K4Q) (Fig. 3*C*).

We previously reported that the Ca^{2+} bowl exerted a force onto the S6 gate of BK(β2) via the calcium bowl site (19), raising the possibility that there may be another pathway in β1, distinct from that in β2. To this end, it is necessary to examine the second calcium binding site mSlo1(D362,D367)of BK channel (9). In other words, the mSlo1(D362,D367)-β1(K3,K4) may play a role in regulating the BK gating similar to that of mSlo1(5D5N)-β2(K33,R34,K35) (26). Contrary to our expectation, we found that their $\Delta\Delta G$ was about 0.1 kcal/mol (Fig. 3*C*), suggesting that there was no significant interaction between the mSlo1(D362,D367) and the β1(K3,K4).

Taken together, there was no electrostatic interaction between the mSlo1 and the β1(K3,K4).

A Strong Hydrophobic Interaction between mSlo1(L906,L908)-β1(L5,V6,M7)—In a separate set of experiments, we found that the three-hydrophobic mutation β1(L5Q,V6Q,M7Q) made a marked shift of +50 mV in V_{50} combined with significant changes in gating kinetics (Table 1), implying that these residues might play a role similar to that of β2(K33,R34,K35) (26). To further identify all of the corresponding hydrophobic sites on mSlo1, that may possibly interact with β1(L5,V6,M7), we scanned all of the hydrophobic residues in the RCK regions of mSlo1 surrounding β1(L5,V6,M7) (Fig. 4*E*) (detailed information is shown in Table 2) and found that the mSlo1(L906,L908), locating behind the calcium bowl, were the only residues possibly interacting with β1(L5,V6,M7). Based on all of the currents as well as the *G-V* curves of mSlo1(L906,L908) *versus* β1(L5,V6,M7) (Fig. 4, *A* and *B*), we noted that the $\Delta\Delta G$ of mSlo1(L906Q,L908Q) *versus* β1 (L5Q,V6Q,M7Q), was significantly larger than 1 kcal/mol in 10, 100, and 300 μM Ca^{2+}, suggesting that the mSlo1(L906,L908) strongly coupled with β1(L5,V6,M7), independent of Ca^{2+}(Fig. 4, *C* and *D*). Moreover, when a substitution of glutamine with alanine (Q→A) was conducted, we found that the $\Delta\Delta G$ of mSlo1(L906A,L908A) *versus* β1(L5A,V6A,M7A) was about 1.3 kcal/mol (Fig. 4*E*), nearly the same as mSlo1(L906Q,L908Q) *versus* β1(L5Q,V6Q,M7Q), whereas no other hydrophobic residues of mSlo1 interact with the β1(L5,V6,M7) with a $\Delta\Delta G \geq 1$ kcal/mol (Fig. 4*E*). Given that the Leu, Met, and Val in both the mSlo1(L906,L908) and β1(L5,V6,M7) have high hydrophobicity, we defined these residues as an H site.

A Putative Structural Model of BK(β1) Channels—As we described the above, both the E and H sites enhanced the calcium sensitivity of BK channels. To further verify their feasibilities in space structure, we constructed a model of BK channel by homology modeling using the known partial crystal structure of BK channels (*i.e.* the published crystal structure of RCK domains) and manually assembled mSlo1 and β1 complex (see "Experimental Procedures"), in which the location of β1(TM1) is placed next to both S1 and S2 of Slo1 (Fig. 5*A*) (29). Based on this information, we noticed in molecular dynamics simulations that the β1(E13,T14) was just located at the top of mSlo1(K392,R393) with a mean distance of about 3.8–4.4 Å in between and that the side chains of three residues β1(L5,V6,M7) were lined in parallel with that of mSlo1(L906,L908), co-localized within close proximity of the residues mSlo1(L906,L908) (Fig. 5*B*). This suggests that the enhancing force by Ca^{2+} binding was possibly coming from H → E → PGD, forming a pathway of enhancing Ca^{2+} sensitivity of BK channels. Along with our experimental results, these simulations led us to suggest that both electrostatic and hydrophobic effects appear to be synergistic for Slo1 α and β1 interactions.

H Site Reducing Magnesium Sensitivity of BK(β1) Channel—Previous studies revealed that the Mg^{2+} binding site was located in the VSD and cytosolic domain (CTD) interface of mSlo1 (7) and that the β1 reduced the Mg^{2+} sensitivity by directly altering the structural configuration of the Mg^{2+} binding site (23). To examine which site, β1(L5,V6,M7) or β1(E13,T14), could affect the Mg^{2+} sensitivity of BK(β1) channels, we performed experiments in a variety of Mg^{2+} concentrations and found that the *G-V* curve showed a leftward shift of 28.5 and 57.1 mV in 10 mM Mg^{2+}, in the presence and absence of β1 subunits, respectively, compared with 0 Mg^{2+} (Fig. 6, *A–C*). This indicates that the β1 reduces the Mg^{2+} sensitivity of BK channels. Here we noticed that the peak currents of BK in Mg^{2+} experiments varied widely due to the blockage of Mg^{2+} while the Mg^{2+} concentrations were elevated. The *G-V* curve showed a leftward shift of 56.7 mV in 10 mM Mg^{2+} in the presence of β1(L5Q,V6Q,M7Q) (Fig. 6, *B* and *C*). Similarly, the *G-V* curve of mSlo1(L906Q,L908Q)-β1 channels had a leftward shift of 50.4 mV. These results suggest that both the mutants β1(L5Q,V6Q,M7Q) and mSlo1(L906Q,L908Q) could eliminate the β1-induced reduction of Mg^{2+} sensitivity of BK(β1) channels. Correspondingly, the *G-V* curve of β1(E13K,T14K) only showed a leftward shift of 30 mV in 10 mM Mg^{2+}, similar to that of the WT β1 (Fig. 6*C*), indicating that the H site but not the E site affected the Mg^{2+} sensitivity of BK(β1) channels (Fig. 6*D*). When Mg^{2+} was increased to 50 mM, we found even

FIGURE 6. **The β1 subunits reducing Mg^{2+} sensitivity of BK-type channels.** *A*, macroscopic currents of all of the BK-type channels were acquired from inside-out patches in 0 (*top*), 10 (middle), and 50 (*bottom*) mM Mg^{2+} at 0 [Ca^{2+}] as indicated. Currents were elicited by 100-ms voltage steps either ranging from −160 to 200 mV in 20-mV increments at 0 and 10 mM [Mg^{2+}] or ranging from −160 to 160 mV in 20-mV increments at 50 mM [Mg^{2+}] after a 20-ms prepulse of −180 mV (only the last 2 ms is shown here) and then returned to a repolarization potential of −120 mV. The data were obtained from the same patch in the presence of 0, 10, and 50 mM [Mg^{2+}]. *B*, the normalized *G-V* curves were plotted for various BK-type channels at 0 (*left*), 10 (middle), and 50 (*right*) mM [Mg^{2+}]. The values of V_{50} are 139.5 ± 5.5 mV (*black*; $n = 9$), 73.4 ± 4.8 mV (*black*; $n = 8$), and 31.0 ± 3.4 mV (*black*; $n = 7$) for mSlo1; 132.7 ± 5.0 mV (*red*; $n = 10$), 103.2 ± 4.8 mV (*red*; $n = 8$), and 57.1.0 ± 4.0 mV (*black*; $n = 8$) for mSlo1-β1; 194.5 ± 7.5 mV (*blue*; $n = 8$), 138.8 ± 4.9 mV (*blue*; $n = 10$), and 83.0 ± 4.5 mV (*black*; $n = 7$) for mSlo1-β1(LVM); 200.6 ± 6.4 mV (*green*; $n = 12$), 150.3 ± 5.1 mV (*green*; $n = 8$), and 77.4 ± 3.3 mV (*black*; $n = 9$) for mSlo1(L906Q,L908Q)-β1; and 188.2 ± 5.7 mV (*pink*; $n = 11$), 134.7 ± 4.9 mV (*pink*; $n = 8$), and 90.5 ± 5.1 mV (*black*; $n = 7$) for mSlo1(L906Q,L908Q) in the presence of 0, 10, and 50 mM Mg^{2+}, respectively. *Corresponding colors* are the same as shown in *A*. *Solid lines* were fitted to the Boltzmann equation under "Experimental Procedures." *C*, the differences of V_{50} between 0 and 10 mM Mg^{2+} (or $\Delta V_{50(0-10\ Mg)}$) were plotted for the BK-type channel as indicated. They are 57 ± 4.5 mV for mSlo1 (*black*; $n = 9$), 29 ± 4 mV for mSlo1-β1 (*red*; $n = 8$), 56 ± 4.3 mV for mSlo1-β1(LVM) (*blue*; $n = 8$), 50 ± 4.2 mV for mSlo1(L906Q,L908Q)-β1 (*green*; $n = 10$), 30 ± 4.1 mV for mSlo1-β1(E13K,T14K) (*dark red*; $n = 11$), and 54 ± 4.8 mV for mSlo1(L906Q,L908Q) (*pink*; $n = 8$), as indicated. *D*, plots of V_{50} *versus* [Mg^{2+}] are shown for mSlo1 (*black*), mSlo1-β1 (*red*), mSlo1-β1(LVM) (*blue*), mSlo1(L906Q,L908Q)-β1 (*green*), and mSlo1(L906Q,L908Q) (*pink*), as indicated. *Error bars*, S.D.

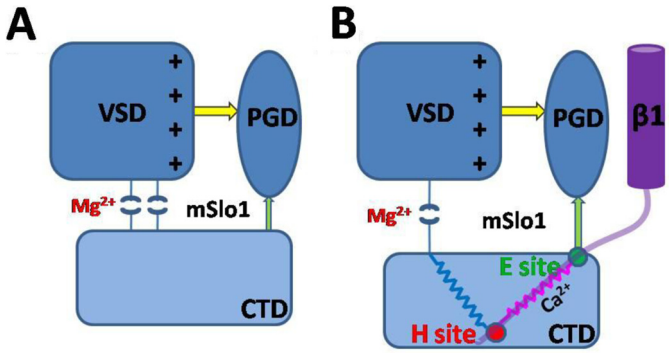

FIGURE 7. **A hypothetical scheme for mechanism of the calcium- and magnesium- and voltage-dependent activation in BK(β1) channels.** The *rounded rectangles* denote the VSD (*dark blue*) and CTD (*light blue*) of mSlo1 (*A*) and mSlo1-β1 (*B*), respectively. The *blue oval* denotes the PGD. The *purple cylinder* denotes the transmembrane domain of β1, and the *light purple curve* denotes the N terminus of β1. *Yellow* and *green arrows* and *pink* and *blue springs* denote the possible interaction pathways. The H site serves as a fixed pulley (*red circle*) transferring the force coming from CTD to enlarge the distance between VSD and CTD to reduce the Mg^{2+} sensitivity, and the E site (*green circle*) then optimizes the direction of the gating force coming from the Ca^{2+} binding sites.

greater leftward shifts of V_{50} (Fig. 6, *A–D*), again demonstrating that only the H site affected the Mg^{2+} sensitivity of BK(β1) channels.

DISCUSSION

BK channels function differently due to their auxiliary β subunits, which underlie their diverse physiological roles in a variety of cells. A lack of detailed structural information of the mSlo1 α-β1 complex has precluded us from fully understanding their coupling mechanisms. It was hypothesized that β1 somehow altered the structural conformation of the Mg^{2+} site to weaken the action of VSD to PGD (Fig. 7*A*) (18). In this study, we demonstrated two complementary pairs of residues located in the CTD, of which the E site only modulated the Ca^{2+} sensitivity, and the H site modulated both the Ca^{2+} and Mg^{2+} sensitivity of BK(β1) channels. Our findings indicated that the H site might play a role as a pivot in transferring a Ca^{2+}-binding force from the calcium bowl in the CTD, which might disturb the structural configuration of the Mg^{2+} site to decrease the Mg^{2+}-binding force onto VSD, ultimately weakening the channel gating. At the same time, the E site served as a scaffold between the membrane-spanning and RCK domains of mSlo1, boosting the force from the H site to enhance channel gating (Fig. 7*B*).

Surprisingly, we found that the H site of β1 was composed of hydrophobic residues, different from the electrostatic site as in β2, although they share similar basic residues at the corresponding position of their N-terminal sequences, indicating that these two subunits have different N-terminal structures. The structure derived from molecular dynamics simulation indicates that the N terminus of β1 has a looplike conformation with no secondary structure, which makes β1(L5,V6,M7) interact with mSlo1(L906/L908) more readily. Unlike the corresponding basic residues β2(K33,R34,K35) the basic residues β1(K3,K4) are located far from the calcium bowl site, suggesting that there is a marked spatial difference in structural arrangement between the N termini of β1 and β2 (26). Given that both the β1 and β2 subunits reduce Mg^{2+} sensitivity (23), we deduce that the perturbation of the Mg^{2+} binding sites ultimately attenuates the Mg^{2+} sensitivity of BK(β1) and BK(β2) channels, because the N termini of β1 and β2 binding to the cytosolic domain may enlarge the distance between VSD and CTD.

In conclusion, we demonstrated that the N terminus of β1 contained an H site in addition to the electrostatic sites as previously described in the N terminus of β2 (26). This novel H site of β1 imparts unique function distinct from that of β2, despite their similar sequences, impacting BK gating with a different mechanism. Additionally, our methods developed in this study may help to further explore how other subunits, such as β3 and β4, differentially regulate the sensitivity of BK channels to divalent ions.

REFERENCES

1. Petersen, O. H., and Maruyama, Y. (1984) Calcium-activated potassium channels and their role in secretion. *Nature* **307,** 693–696
2. Brayden, J. E., and Nelson, M. T. (1992) Regulation of arterial tone by activation of calcium-dependent potassium channels. *Science* **256,** 532–535
3. Fuchs, P. A., and Murrow, B. W. (1992) Cholinergic inhibition of short (outer) hair cells of the chick's cochlea. *J. Neurosci.* **12,** 800–809
4. Robitaille, R., and Charlton, M. P. (1992) Presynaptic calcium signals and transmitter release are modulated by calcium-activated potassium channels. *J. Neurosci.* **12,** 297–305
5. Wu, Y. C., Ricci, A. J., and Fettiplace, R. (1999) Two components of transducer adaptation in auditory hair cells. *J. Neurophysiol.* **82,** 2171–2181
6. McManus, O. B., and Magleby, K. L. (1991) Accounting for the Ca^{2+}-dependent kinetics of single large-conductance Ca^{2+}-activated K^+ channels in rat skeletal muscle. *J. Physiol.* **443,** 739–777
7. Yang, H., Shi, J., Zhang, G., Yang, J., Delaloye, K., and Cui, J. (2008) Activation of Slo1 BK channels by Mg^{2+} coordinated between the voltage sensor and RCK1 domains. *Nat. Struct. Mol. Biol.* **15,** 1152–1159
8. Schreiber, M., and Salkoff, L. (1997) A novel calcium-sensing domain in the BK channel. *Biophys. J.* **73,** 1355–1363
9. Xia, X. M., Zeng, X., and Lingle, C. J. (2002) Multiple regulatory sites in large-conductance calcium-activated potassium channels. *Nature* **418,** 880–884
10. Shi, J., Krishnamoorthy, G., Yang, Y., Hu, L., Chaturvedi, N., Harilal, D., Qin, J., and Cui, J. (2002) Mechanism of magnesium activation of calcium-activated potassium channels. *Nature* **418,** 876–880
11. Tanaka, Y., Meera, P., Song, M., Knaus, H. G., and Toro, L. (1997) Molecular constituents of maxi KCa channels in human coronary smooth muscle: predominant α + β subunit complexes. *J. Physiol.* **502,** 545–557
12. Brenner, R., Peréz, G. J., Bonev, A. D., Eckman, D. M., Kosek, J. C., Wiler, S. W., Patterson, A. J., Nelson, M. T., and Aldrich, R. W. (2000) Vasoregulation by the beta1 subunit of the calcium-activated potassium channel. *Nature* **407,** 870–876
13. Plüger, S., Faulhaber, J., Furstenau, M., Lohn, M., Waldschütz, R., Gollasch, M., Haller, H., Luft, F. C., Ehmke, H., and Pongs, O. (2000) Mice with disrupted BK channel beta1 subunit gene feature abnormal Ca^{2+} spark/STOC coupling and elevated blood pressure. *Circ. Res.* **87,** E53–E60
14. Behrens, R., Nolting, A., Reimann, F., Schwarz, M., Waldschütz, R., and Pongs, O. (2000) hKCNMB3 and hKCNMB4, cloning and characterization of two members of the large-conductance calcium-activated potassium channel beta subunit family. *FEBS Lett.* **474,** 99–106
15. Brenner, R., Jegla, T. J., Wickenden, A., Liu, Y., and Aldrich, R. W. (2000) Cloning and functional characterization of novel large conductance calcium-activated potassium channel β subunits, hKCNMB3 and hKCNMB4. *J. Biol. Chem.* **275,** 6453–6461
16. Meera, P., Wallner, M., and Toro, L. (2000) A neuronal beta subunit (KCNMB4) makes the large conductance, voltage- and Ca^{2+}-activated K^+ channel resistant to charybdotoxin and iberiotoxin. *Proc. Natl. Acad. Sci.*

U.S.A. **97,** 5562–5567
17. Uebele, V. N., Lagrutta, A., Wade, T., Figueroa, D. J., Liu, Y., McKenna, E., Austin, C. P., Bennett, P. B., and Swanson, R. (2000) Cloning and functional expression of two families of β-subunits of the large conductance calcium-activated K^+ channel. *J. Biol. Chem.* **275,** 23211–23218
18. Hu, L., Shi, J., Ma, Z., Krishnamoorthy, G., Sieling, F., Zhang, G., Horrigan, F. T., and Cui, J. (2003) Participation of the S4 voltage sensor in the Mg^{2+}-dependent activation of large conductance (BK) K^+ channels. *Proc. Natl. Acad. Sci. U.S.A.* **100,** 10488–10493
19. Ding, J. P., Li, Z. W., and Lingle, C. J. (1998) Inactivating BK channels in rat chromaffin cells may arise from heteromultimeric assembly of distinct inactivation-competent and noninactivating subunits. *Biophys. J.* **74,** 268–289
20. Wang, Y. W., Ding, J. P., Xia, X. M., and Lingle, C. J. (2002) Consequences of the stoichiometry of Slo1 α and auxiliary beta subunits on functional properties of large-conductance Ca^{2+}-activated K^+ channels. *J. Neurosci.* **22,** 1550–1561
21. Lee, U. S., and Cui, J. (2010) BK channel activation: structural and functional insights. *Trends Neurosci.* **33,** 415–423
22. Qian, X., and Magleby, K. L. (2003) Beta1 subunits facilitate gating of BK channels by acting through the Ca^{2+}, but not the Mg^{2+}, activating mechanisms. *Proc. Natl. Acad. Sci. U.S.A.* **100,** 10061–10066
23. Sun, X., Shi, J., Delaloye, K., Yang, X., Yang, H., Zhang, G., and Cui, J. (2013) The interface between membrane-spanning and cytosolic domains in Ca^{2+}-dependent K^+ channels is involved in β subunit modulation of gating. *J. Neurosci.* **33,** 11253–11261
24. Zeng, X. H., Xia, X. M., and Lingle, C. J. (2003) Redox-sensitive extracellular gates formed by auxiliary β subunits of calcium-activated potassium channels. *Nat. Struct. Biol.* **10,** 448–454
25. Chen, M., Gan, G., Wu, Y., Wang, L., Wu, Y., and Ding, J. (2008) Lysine-rich extracellular rings formed by hβ2 subunits confer the outward rectification of BK channels. *PLoS One* **3,** e2114
26. Hou, P., Zeng, W., Gan, G., Lv, C., Guo, X., Zhang, Z., Liu, H., Wu, Y., Yao, J., Wei, A. D., Wang, S., and Ding, J. (2013) Inter-α/β subunits coupling mediating pre-inactivation and augmented activation of BKCa(β2). *Sci. Rep.* **3,** 1666
27. Wallner, M., Meera, P., and Toro, L. (1996) Determinant for β-subunit regulation in high-conductance voltage-activated and Ca^{2+}-sensitive K^+ channels: an additional transmembrane region at the N terminus. *Proc. Natl. Acad. Sci. U.S.A.* **93,** 14922–14927
28. Morrow, J. P., Zakharov, S. I., Liu, G., Yang, L., Sok, A. J., and Marx, S. O. (2006) Defining the BK channel domains required for β1-subunit modulation. *Proc. Natl. Acad. Sci. U.S.A.* **103,** 5096–5101
29. Liu, G., Zakharov, S. I., Yang, L., Wu, R. S., Deng, S. X., Landry, D. W., Karlin, A., and Marx, S. O. (2008) Locations of the β1 transmembrane helices in the BK potassium channel. *Proc. Natl. Acad. Sci. U.S.A.* **105,** 10727–10732
30. Orio, P., Torres, Y., Rojas, P., Carvacho, I., Garcia, M. L., Toro, L., Valverde, M. A., and Latorre, R. (2006) Structural determinants for functional coupling between the β and α subunits in the Ca^{2+}-activated K^+ (BK) channel. *J. Gen. Physiol.* **127,** 191–204
31. Wu, Y., Yang, Y., Ye, S., and Jiang, Y. (2010) Structure of the gating ring from the human large-conductance Ca^{2+}-gated K^+ channel. *Nature* **466,** 393–397
32. Yuan, P., Leonetti, M. D., Pico, A. R., Hsiung, Y., and MacKinnon, R. (2010) Structure of the human BK channel Ca^{2+}-activation apparatus at 3.0 Å resolution. *Science* **329,** 182–186
33. Case, D. A., Darden, T. A., Cheatham, T. E., 3rd, Simmerling, C. L., Wang, J., Duke, R. E., Luo, R., Walker, R. C., Zhang, W., Merz, K. M., Roberts, B., Hayik, S., Roitberg, A., Seabra, G., Swails, J., Goetz, A. W., Kolossváry, I., Wong, K. F., Paesani, F., Vanicek, J., Wolf, R. M., Liu, J., Wu, X., Brozell, S. R., Steinbrecher, T., Gohlke, H., Cai, Q., Ye, X., Wang, J., Hsieh, M. J., Cui, G., Roe, D. R., Mathews, D. H., Seetin, M. G., Salomon-Ferrer, R., Sagui, C., Babin, V., Luchko, T., Gusarov, S., Kovalenko, A., and Kollman, P. A. (2012) *AMBER*, University of California, San Francisco
34. McManus, O. B., Helms, L. M., Pallanck, L., Ganetzky, B., Swanson, R., and Leonard, R. J. (1995) Functional role of the β subunit of high conductance calcium-activated potassium channels. *Neuron* **14,** 645–650
35. Nimigean, C. M., and Magleby, K. L. (1999) The β subunit increases the Ca^{2+} sensitivity of large conductance Ca^{2+}-activated potassium channels by retaining the gating in the bursting states. *J. Gen. Physiol.* **113,** 425–440
36. Xia, X. M., Ding, J. P., and Lingle, C. J. (1999) Molecular basis for the inactivation of Ca^{2+}- and voltage-dependent BK channels in adrenal chromaffin cells and rat insulinoma tumor cells. *J. Neurosci.* **19,** 5255–5264
37. Wallner, M., Meera, P., and Toro, L. (1999) Molecular basis of fast inactivation in voltage and Ca^{2+}-activated K+ channels: a transmembrane β-subunit homolog. *Proc. Natl. Acad. Sci. U.S.A.* **96,** 4137–4142
38. Carter, P. J., Winter, G., Wilkinson, A. J., and Fersht, A. R. (1984) The use of double mutants to detect structural changes in the active site of the tyrosyl-tRNA synthetase (*Bacillus stearothermophilus*). *Cell* **38,** 835–840
39. Serrano, L., Horovitz, A., Avron, B., Bycroft, M., and Fersht, A. R. (1990) Estimating the contribution of engineered surface electrostatic interactions to protein stability by using double-mutant cycles. *Biochemistry* **29,** 9343–9352
40. Yifrach, O., and MacKinnon, R. (2002) Energetics of pore opening in a voltage-gated K^+ channel. *Cell* **111,** 231–239
41. Sadovsky, E., and Yifrach, O. (2007) Principles underlying energetic coupling along an allosteric communication trajectory of a voltage-activated K^+ channel. *Proc. Natl. Acad. Sci. U.S.A.* **104,** 19813–19818